Table 7.3.5a: Measured results for sample P45075A, G00 tilt.

Sample P45075A G00 tilt	**Parameter**	**P1 d_R=211.3mm**	**P2 d_R=215.3mm**	**P3 d_R=220.6mm**
Experiment	**N(points)**	6234	9609	14194
	Δz(mm)	0.450	0.397	0.379
	A(mm^2)	283.6	280.4	277.16
2D fitting	**K_B(rad)**	$-3.450\ 10^{-3}$	$-2.208\ 10^{-3}$	$-1.142\ 10^{-3}$
	r_B^2	0.9999959	0.9999951	0.9999955
	K_C(rad)	$-4.557\ 10^{-3}$	$-3.303\ 10^{-3}$	$-2.062\ 10^{-3}$
	r_C^2	0.9999638	0.9999613	0.9999516
	R_B(mm)	204.1	204.2	204.3
	R_C(mm)	160.8	160.8	160.9
3D fitting	**R_B(mm)**	204.2	204.2	204.6
	R_C(mm)	160.8	160.7	160.4
	σ_B(mm)	$4.5\ 10^{-3}$	$3.5\ 10^{-3}$	$4.6\ 10^{-3}$
	σ_C(mm)	$8.9\ 10^{-3}$	$6.5\ 10^{-3}$	$7.5\ 10^{-3}$
	x_0(mm)	0.729	0.459	0.442
	y_0(mm)	-0.720	-0.508	-0.488
	σ_{Xo}(mm)	$1.1\ 10^{-4}$	$7.1\ 10^{-5}$	$8.4\ 10^{-5}$
	σ_{Yo}(mm)	$7.5\ 10^{-5}$	$5.3\ 10^{-5}$	$6.6\ 10^{-5}$
	θ(°)	0.50	0.62	0.44
	σ_θ(°)	$3.7\ 10^{-3}$	$2.8\ 10^{-3}$	$3.6\ 10^{-3}$
	r^2	0.9999974	0.9999974	0.9999936
	$\Delta z_{RESIDUAL}$(mm)	0.420	0.424	0.438

Möller-Wedel radioscope measurement: **R_B= 201.4±1mm**

R_C= 159.8±1mm

Fig. 7.3.5a: Measured surface topographies and residuals: sample P45075A,G00 tilt.

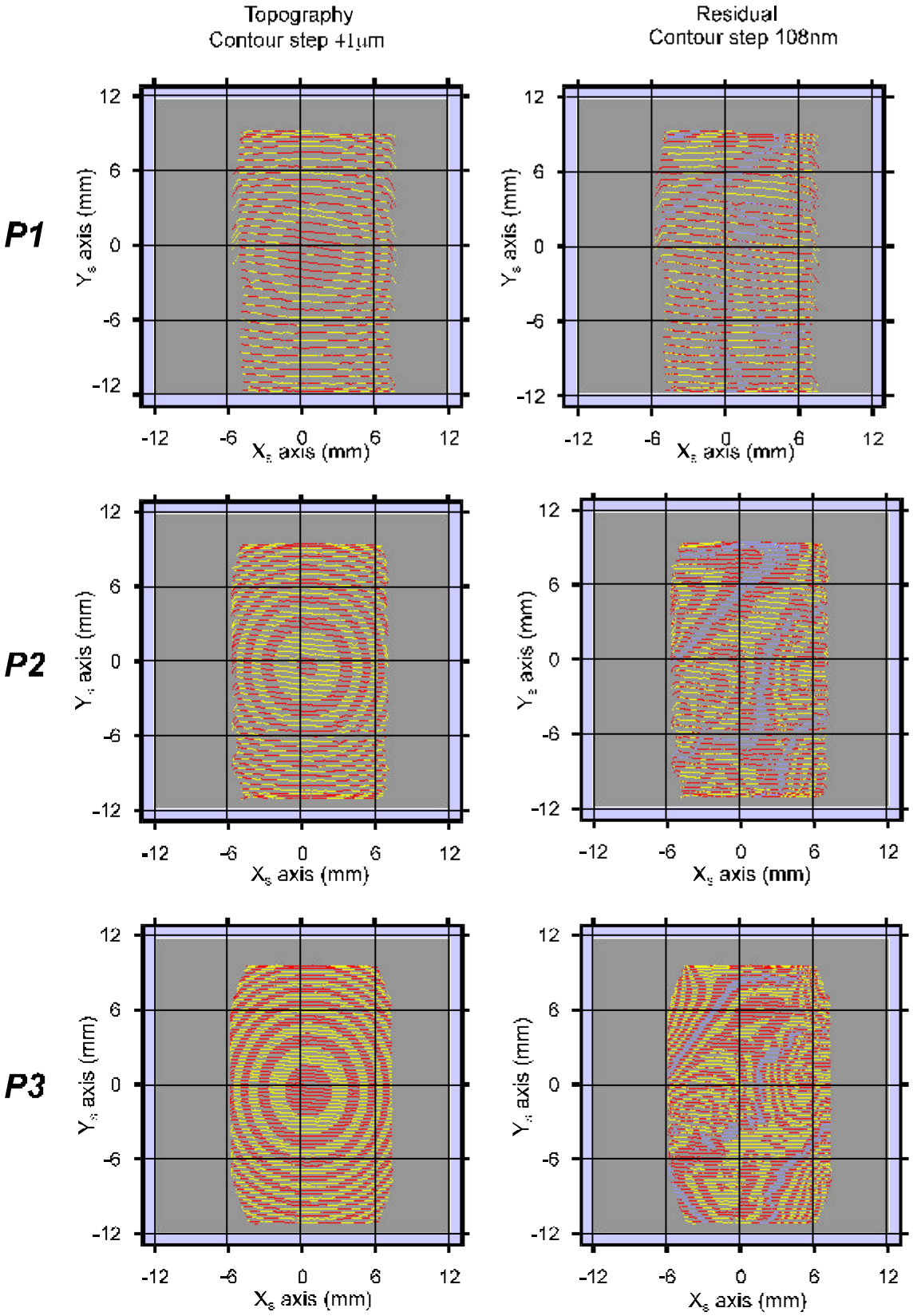

Table 7.3.5b: Measured results for sample P45075A, G30 tilt.

Sample P45075A G30 tilt	Parameter	P1 d_R=211.3mm	P2 d_R=215.3mm	P3 d_R=220.6mm
Experiment	N(points)	11404	15008	18048
	Dz(mm)	0.537	0.526	0.488
	A(mm^2)	424.3	405.4	380.2
2D fitting	K_B(rad)	$8.692\ 10^{-4}$	$-1.142\ 10^{-3}$	$-4.291\ 10^{-3}$
	r_B^2	0.9999961	0.9999550	0.9999954
	K_C(rad)	$-2.558\ 10^{-3}$	$-2.062\ 10^{-3}$	$-1.790\ 10^{-3}$
	r_C^2	0.9999589	0.9999516	0.9999413
	R_B(mm)	204.2	204.3	204.4
	R_C(mm)	160.8	160.9	161.0
3D fitting	R_B(mm)	203.9	203.9	204.5
	R_C(mm)	160.6	160.5	160.4
	s_B(mm)	$3.3\ 10^{-3}$	$3.4\ 10^{-3}$	$3.6\ 10^{-3}$
	s_C(mm)	$5.6\ 10^{-3}$	$6.0\ 10^{-3}$	$5.3\ 10^{-3}$
	x_0(mm)	0.193	0.246	0.289
	y_0(mm)	-0.412	-0.333	-0.100
	s_{Xo}(mm)	$5.6\ 10^{-5}$	$5.5\ 10^{-5}$	$5.8\ 10^{-5}$
	s_{Yo}(mm)	$6.6\ 10^{-5}$	$6.9\ 10^{-5}$	$5.8\ 10^{-5}$
	q(°)	29.4	29.4	29.2
	s_q(°)	$3.8\ 10^{-3}$	$3.9\ 10^{-3}$	$3.9\ 10^{-3}$
	r^2	0.9999972	0.999996	0.9999960
	$Dz_{RESIDUAL}$(mm)	0.514	0.520	0.455

Möller-Wedel radioscope measurement: **R_B= 201.4±1mm**

R_C= 159.8±1mm

Fig. 7.3.5b: Measured surface topographies and residuals: sample P45075A, G30 tilt.

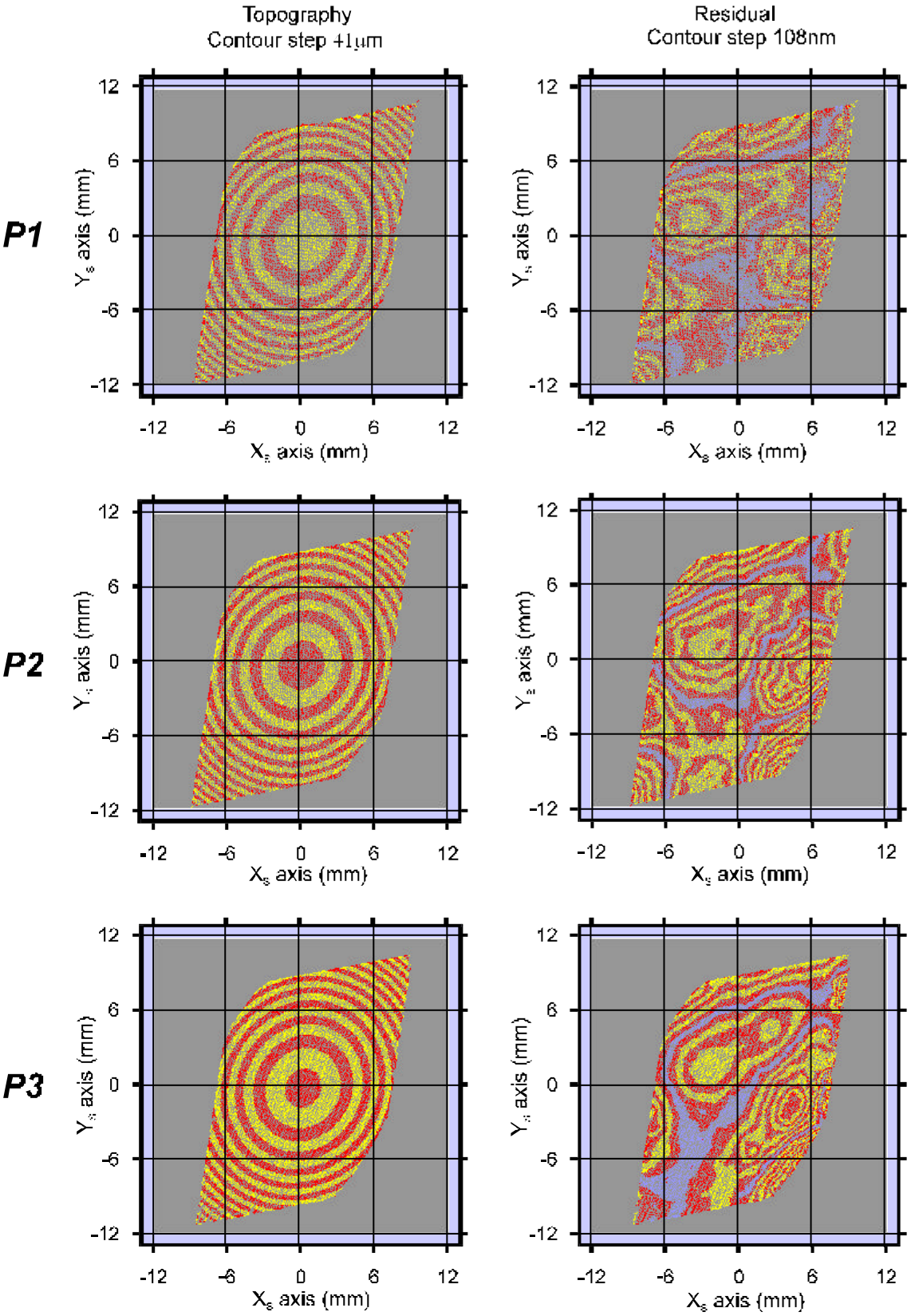

Table 7.3.5c: Measured results for sample P45075A, G60 tilt.

Sample P45075A G60 tilt	Parameter	P1 d_R=211.3mm	P2 d_R=215.3mm	P3 d_R=220.6mm
Experiment	N(points)	11768	15070	18728
	Dz(mm)	0.513	0.541	0.489
	A(mm^2)	414.3	412.9	387.1
2D fitting	K_B(rad)	$1.678\ 10^{-4}$	$1.773\ 10^{-3}$	$2.9315\ 10^{-4}$
	r_B^2	0.9999958	0.9999952	0.9999955
	K_C(rad)	$2.142\ 10^{-3}$	$3.788\ 10^{-3}$	$2.850\ 10^{-3}$
	r_C^2	0.9999958	0.9999564	0.9999506
	R_B(mm)	204.1	204.1	204.2
	R_C(mm)	161.0	161.2	161.2
3D fitting	R_B(mm)	204.1	204.0	204.2
	R_C(mm)	160.2	160.2	160.4
	s_B(mm)	$2.8\ 10^{-3}$	$2.77\ 10^{-3}$	$3.2\ 10^{-3}$
	s_C(mm)	$4.2\ 10^{-3}$	$4.41\ 10^{-3}$	$5.3\ 10^{-3}$
	x_0(mm)	-0.347	0.589	-0.442
	y_0(mm)	0.036	0.365	0.060
	s_{Xo}(mm)	$5.3\ 10^{-5}$	$5.9\ 10^{-5}$	$7.4\ 10^{-5}$
	s_{Yo}(mm)	$4.2\ 10^{-5}$	$4.7\ 10^{-5}$	$4.6\ 10^{-5}$
	q(°)	59.64	59.41	59.34
	s_q(°)	$3.1\ 10^{-3}$	$3.1\ 10^{-3}$	$3.8\ 10^{-3}$
	r^2	0.9999981	0.9999977	0.9999968
	$Dz_{RESIDUAL}$(mm)	$7.02\ 10^{-4}$	$7.16\ 10^{-4}$	$8.54\ 10^{-4}$

Möller-Wedel radioscope measurement: **R_B= 201.4±1mm**

R_C= 159.8±1mm

Fig. 7.3.5c: Measured surface topographies and residuals: sample P45075A, G60 tilt.

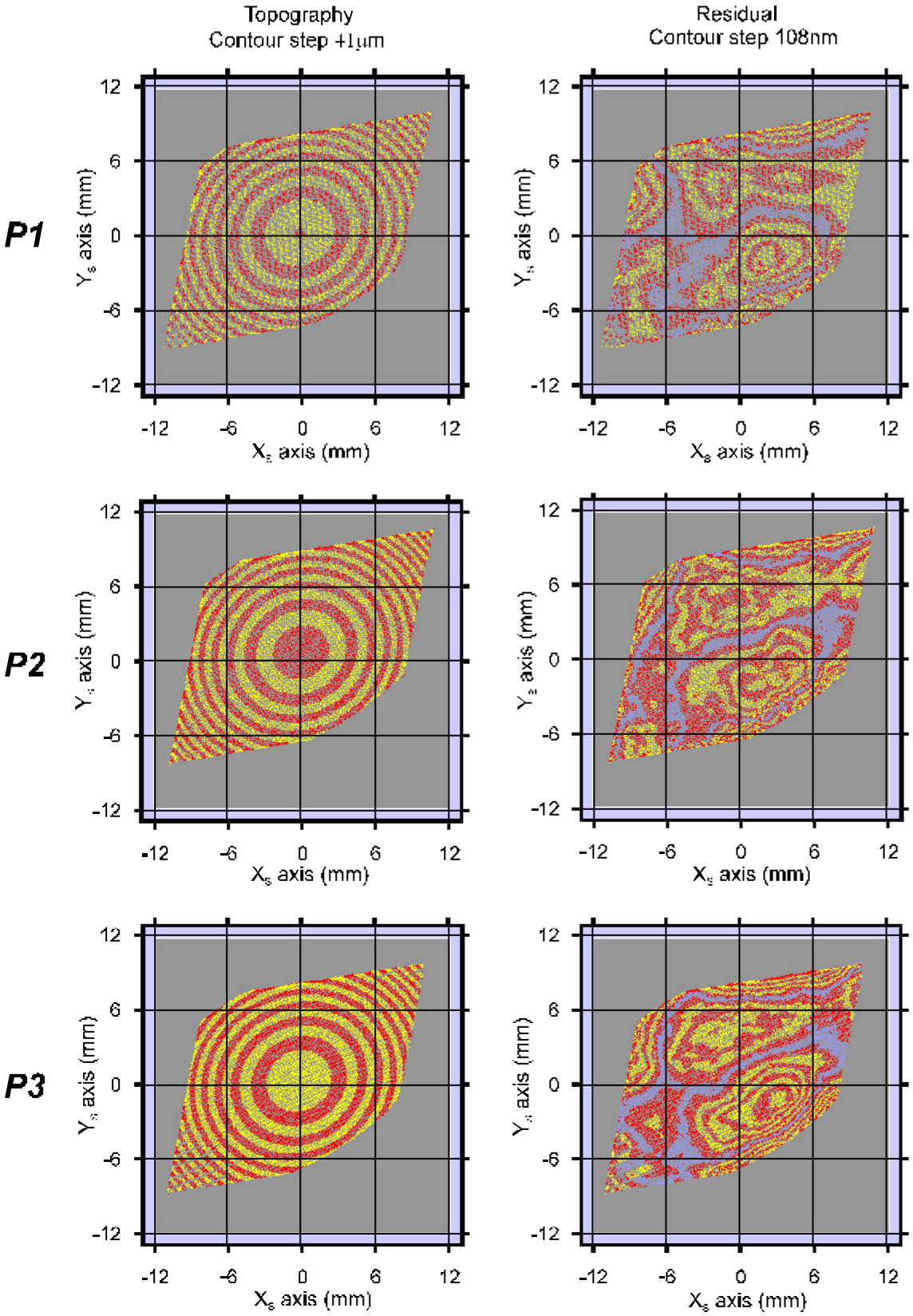

Table 7.3.5d: Measured results for sample P45075A, G90 tilt.

Sample P45075A G90 tilt	Parameter	P1 d_R=211.3mm	P2 d_R=215.3mm	P3 d_R=220.6mm
Experiment	N(points)	6517	9553	13569
	Δz(mm)	0.393	0.588	0.414
	A(mm^2)	270.5	267.9	259.2
2D fitting	K_B(rad)	2.927 10^{-3}	3.154 10^{-3}	3.109 10^{-3}
	r_B^2	0.9999947	0.9999967	0.9999973
	K_C(rad)	2.703 10^{-3}	2.495 10^{-3}	2.737 10^{-3}
	r_C^2	0.9999715	0.9999758	0.9999733
	R_B(mm)	203.8	203.9	204.1
	R_C(mm)	161.1	161.2	161.4
3D fitting	R_B(mm)	202.8	203.4	203.6
	R_C(mm)	161.1	161.0	161.0
	σ_B(mm)	1.087 10^{-2}	3.6 10^{-3}	3.7 10^{-3}
	σ_C(mm)	1.598 10^{-2}	5.2 10^{-3}	5.3 10^{-3}
	x_0(mm)	-0.596	-0.639	-0.637
	y_0(mm)	0.430	0.416	0.452
	σ_{Xo}(mm)	1.5 10^{-4}	4.8 10^{-5}	4.9 10^{-5}
	σ_{Yo}(mm)	2.1 10^{-4}	7.2 10^{-5}	7.5 10^{-5}
	θ(°)	89.59	89.46	89.43
	σ_θ(°)	8.3 10^{-3}	2.7 10^{-3}	2.8 10^{-3}
	r^2	0.9999864	0.9999979	0.9999969
	$\Delta z_{RESIDUAL}$(mm)	1.627 10^{-3}	5.838 10^{-4}	7.193 10^{-4}

Möller-Wedel radioscope measurement: **R_B= 201.4±1mm**

R_C= 159.8±1mm

Fig. 7.3.5d: Measured surface topographies and residuals: sample P45075A,G90 tilt.

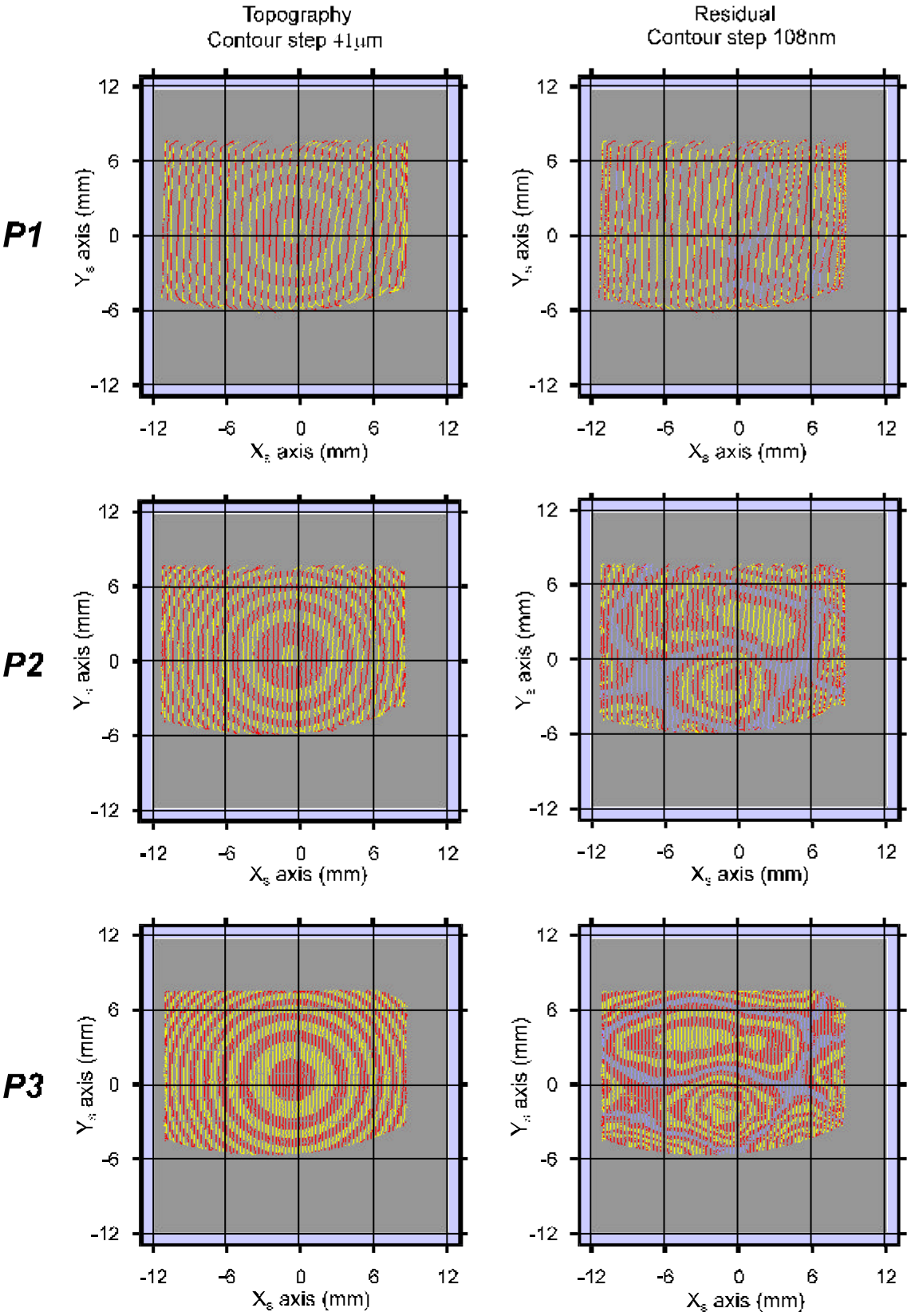

Table 7.3.6a: Measured results for sample P45075B, G00 tilt.

Sample P45075B G00 tilt	Parameter	P1 d_R=211.3mm	P2 d_R=215.3mm	P3 d_R=220.6mm
Experiment	N(points)	6768	9547	14392
	Dz(mm)	0.419	0.424	0.438
	A(mm^2)	274.6	272.3	269.7
2D fitting	K_B(rad)	$-2.681\ 10^{-3}$	$-5.769\ 10^{-3}$	$-6.017\ 10^{-3}$
	r_B^2	0.9999890	0.9999875	0.9999910
	K_C(rad)	$-8.891\ 10^{-4}$	$-3.121\ 10^{-3}$	$-6.012\ 10^{-3}$
	r_C^2	0.9999885	0.9999860	0.9999778
	R_B(mm)	203.3	203.5	203.7
	R_C(mm)	160.1	160.2	160.3
3D fitting	R_B(mm)	204.2	204.5	204.4
	R_C(mm)	159.9	159.7	159.7
	s_B(mm)	$7.0\ 10^{-3}$	$5.3\ 10^{-3}$	$5.0\ 10^{-3}$
	s_C(mm)	$1.2\ 10^{-2}$	$9.4\ 10^{-3}$	$8.2\ 10^{-3}$
	x_0(mm)	0.140	0.510	0.991
	y_0(mm)	-0.575	-1.203	-1.249
	s_{Xo}(mm)	$1.4\ 10^{-4}$	$1.4\ 10^{-4}$	$1.3\ 10^{-4}$
	s_{Yo}(mm)	$9.3\ 10^{-5}$	$7.4\ 10^{-5}$	$8.3\ 10^{-5}$
	q(°)	0.21	0.04	0.14
	s_q(°)	$5.3\ 10^{-3}$	$4.2\ 10^{-3}$	$3.9\ 10^{-3}$
	r^2	0.9999932	0.9999949	0.99999372
	$Dz_{RESIDUAL}$(mm)	$1.106\ 10^{-3}$	$1.047\ 10^{-3}$	$1.227\ 10^{-3}$

Möller-Wedel radioscope measurement: **R_B= 202.7±1mm**

R_C= 158.0±1mm

Fig. 7.3.6a: Measured surface topographies and residuals: sample P45075B,G00 tilt.

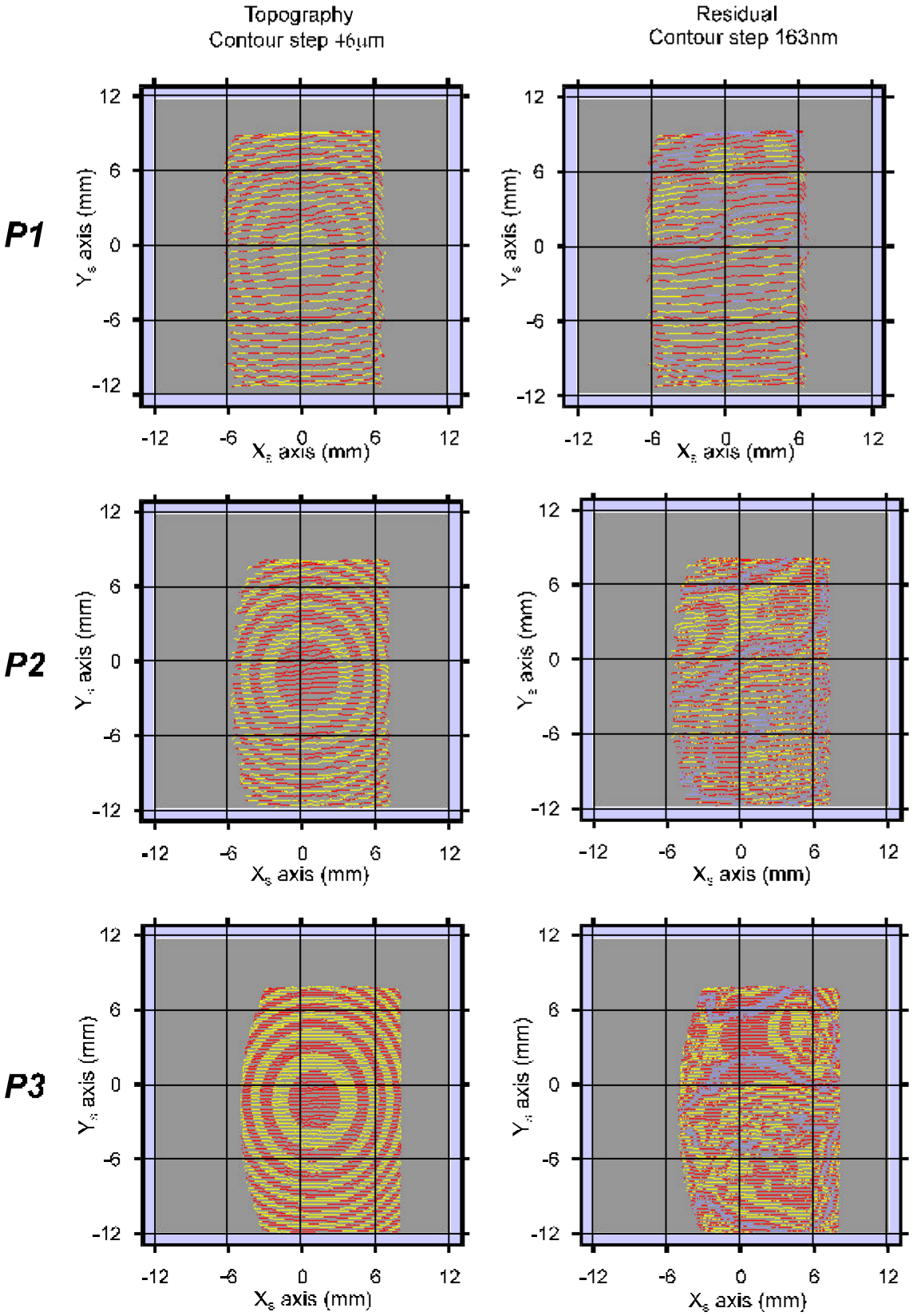

Table 7.3.6b: Measured results for sample P45075B, G30 tilt.

P45075B sample G30 tilt	Parameter	P1 d_R=211.3mm	P2 d_R=215.3mm	P3 d_R=220.6mm
Experiment	N(points)	11665	15499	18694
	Dz(mm)	0.514	0.519	0.454
	A(mm^2)	396.9	390.9	365.8
2D fitting	K_B(rad)	$8.273\ 10^{-4}$	$9.293\ 10^{-4}$	$-4.632\ 10^{-4}$
	r_B^2	0.99999178	0.9999897	0.9999906
	K_C(rad)	$-3.263\ 10^{-3}$	$-5.557\ 10^{-3}$	$7.883\ 10^{-3}$
	r_C^2	0.9999875	0.9999901	0.999972
	R_B(mm)	203.4	203.5	203.6
	R_C(mm)	160.1	160.2	160.2
3D fitting	R_B(mm)	203.4	203.6	204.1
	R_C(mm)	159.5	159.8	158.5
	s_B(mm)	$6.4\ 10^{-3}$	$5.5\ 10^{-3}$	$6.8\ 10^{-3}$
	s_C(mm)	$1.1\ 10^{-2}$	$9.9\ 10^{-3}$	$9.4\ 10^{-3}$
	x_0(mm)	0.537	0.899	-1.221
	y_0(mm)	-0.151	-0.170	0.105
	s_{Xo}(mm)	$1.3\ 10^{-4}$	$1.2\ 10^{-4}$	$1.2\ 10^{-4}$
	s_{Yo}(mm)	$1.1\ 10^{-4}$	$1.2\ 10^{-4}$	$1.3\ 10^{-4}$
	q(°)	29.96	29.98	29.32
	s_q(°)	$7.4\ 10^{-3}$	$6.5\ 10^{-3}$	$6.8\ 10^{-3}$
	r^2	0.9999890	0.9999892	0.9999882
	$Dz_{RESIDUAL}$(mm)	$1.568\ 10^{-3}$	$1.801\ 10^{-3}$	$1.525\ 10^{-3}$

Möller-Wedel radioscope measurement: **R_B= 202.7±1mm**

R_C= 158.0±1mm

Fig. 7.3.6b: Measured surface topographies and residuals: sample P45075B, G30 tilt.

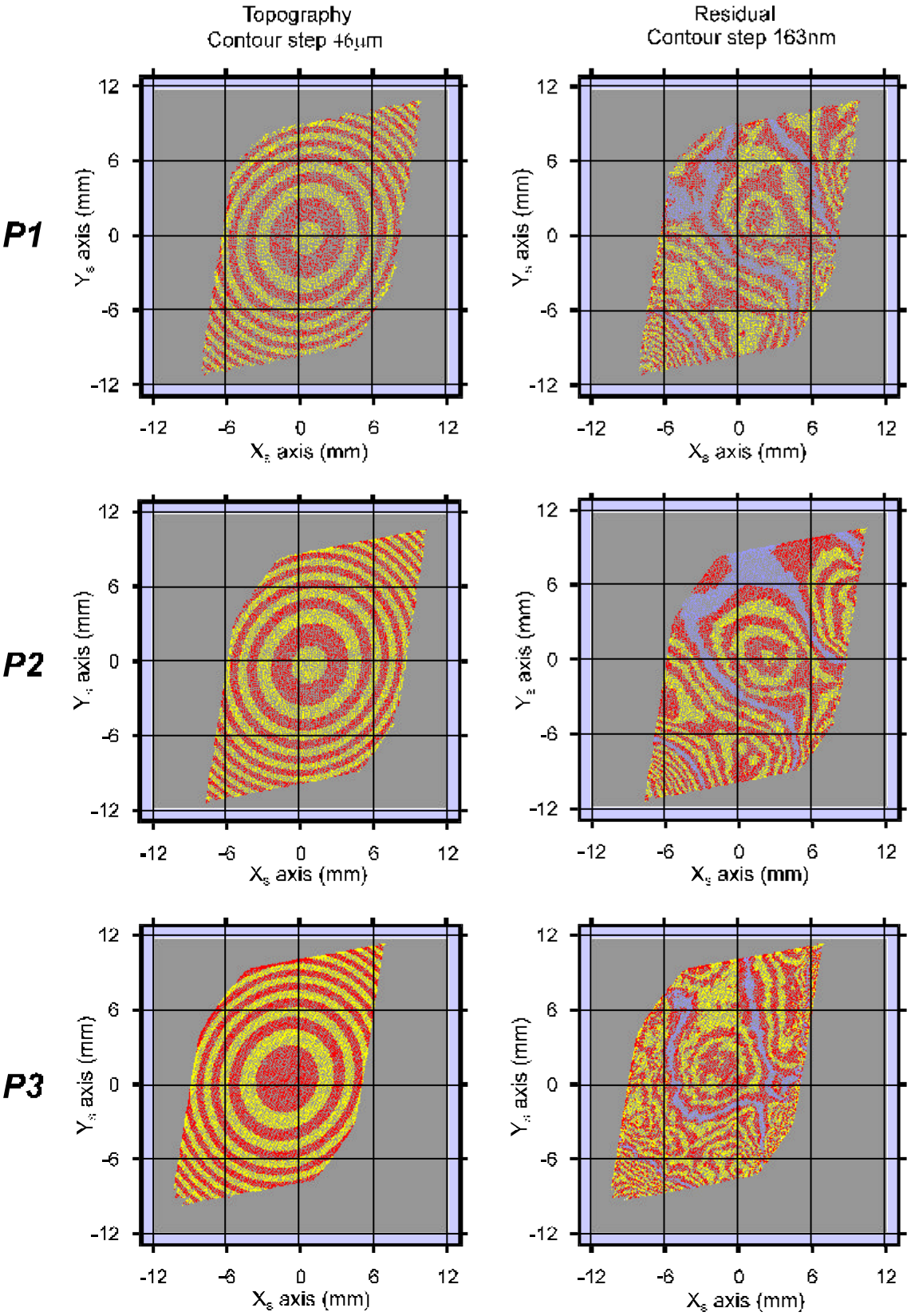

Table 7.3.6c: Measured results for sample P45075B, G60 tilt.

P45075B sample G60 tilt	Parameter	P1 d_R=211.3mm	P2 d_R=215.3mm	P3 d_R=220.6mm
Experiment	N(points)	11527	15088	19251
	Δz(mm)	0.507	0.514	0.470
	A(mm^2)	390.7	392.3	373.0
2D fitting	K_B(rad)	$-2.001\ 10^{-3}$	$2.084\ 10^{-3}$	$2.010\ 10^{-3}$
	r_B^2	0.9999915	0.9999476	0.9999920
	K_C(rad)	$1.475\ 10^{-3}$	$3.420\ 10^{-3}$	$2.145\ 10^{-3}$
	r_C^2	0.9999842	0.9999716	0.9999766
	R_B(mm)	203.4	203.3	203.6
	R_C(mm)	160.4	160.4	160.5
3D fitting	R_B(mm)	203.4	203.4	203.4
	R_C(mm)	160.0	160.0	159.4
	σ_B(mm)	$5.4\ 10^{-3}$	$3.9\ 10^{-3}$	$4.2\ 10^{-3}$
	σ_C(mm)	$8.2\ 10^{-3}$	$6.0\ 10^{-3}$	$7.2\ 10^{-3}$
	x_0(mm)	-0.208	0.537	0.310
	y_0(mm)	0.424	0.370	0.401
	σ_{Xo}(mm)	$1.2\ 10^{-4}$	$7.9\ 10^{-5}$	$1.2\ 10^{-4}$
	σ_{Yo}(mm)	$7.8\ 10^{-5}$	$6.3\ 10^{-3}$	$6.3\ 10^{-5}$
	θ(°)	60.05	61.11	59.85
	σ_θ(°)	$6.0\ 10^{-3}$	$4.1\ 10^{-3}$	$5.0\ 10^{-3}$
	r^2	0.9999932	0.9999956	0.999995
	$\Delta z_{RESIDUAL}$(mm)	$1.100\ 10^{-3}$	$1.413\ 10^{-3}$	$1.046\ 10^{-3}$

Möller-Wedel radioscope measurement: **R_B= 202.7±1mm**

R_C= 158.0±1mm

Fig. 7.3.6c: Measured surface topographies and residuals: sample P45075B, G60 tilt.

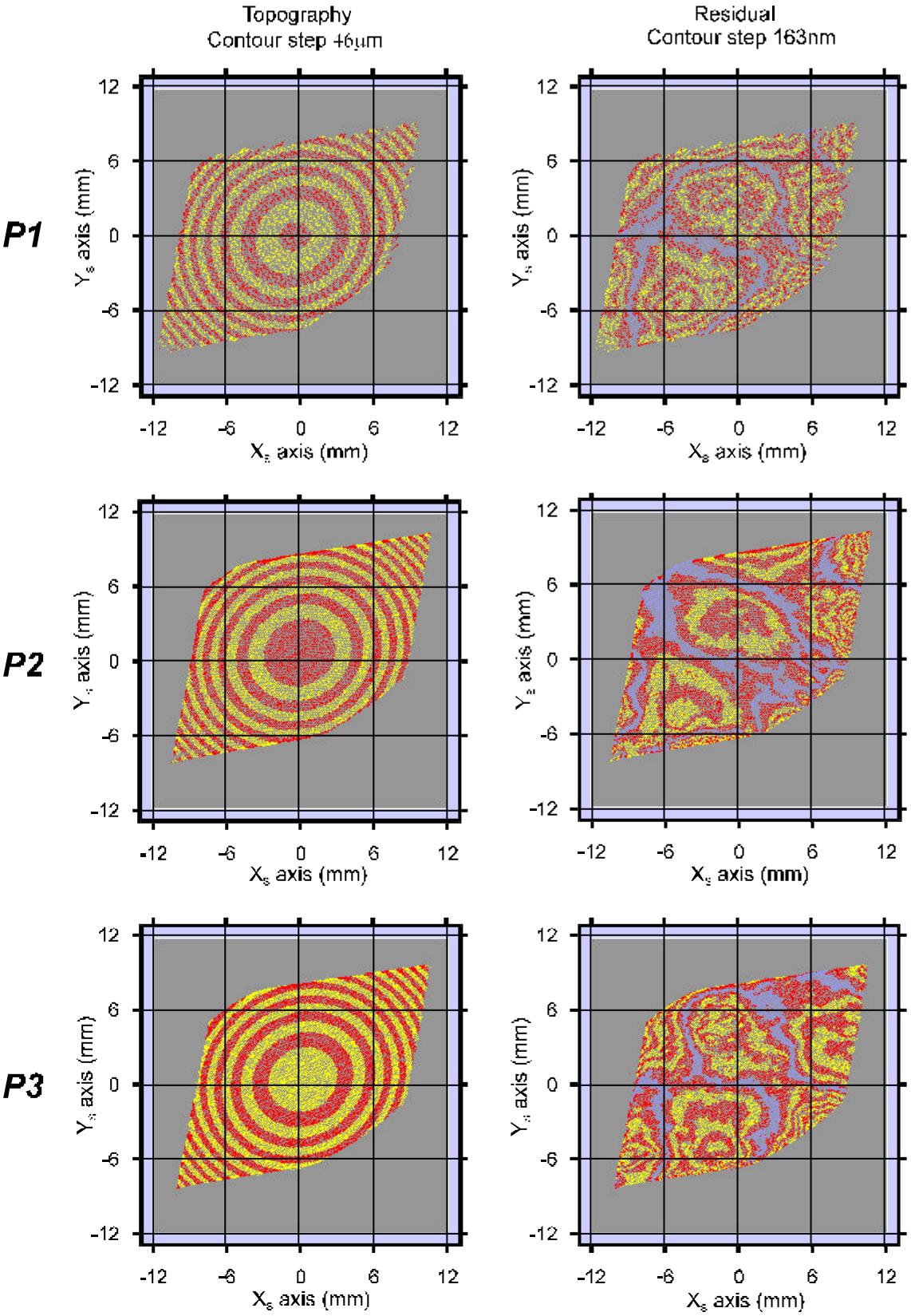

Table 7.3.6d: Measured results for sample P45075B, G90 tilt.

Sample P45075B G90 tilt	Parameter	P1 d_R=211.3mm	P2 d_R=215.3mm	P3 d_R=220.6mm
Experiment	N(points)	6517	9553	13569
	Dz(mm)	0.393	0.588	0.414
	A(mm^2)	270.5	268.0	259.2
2D fitting	K_B(rad)	$-9.927\ 10^{-3}$	$2.393\ 10^{-3}$	$2.886\ 10^{-3}$
	r_B^2	0.9999938	0.9999493	0.9999948
	K_C(rad)	$2.582\ 10^{-3}$	$3.643\ 10^{-3}$	$5.981\ 10^{-3}$
	r_C^2	0.9999874	0.9999815	0.9999854
	R_B(mm)	203.3	203.4	203.6
	R_C(mm)	160.5	160.8	160.9
3D fitting	R_B(mm)	202.7	203.4	204.4
	R_C(mm)	160.5	160.7	161.1
	s_B(mm)	$8.0\ 10^{-3}$	$1.2\ 10^{-2}$	$1.6\ 10^{-2}$
	s_C(mm)	$1.2\ 10^{-2}$	$1.7\ 10^{-2}$	$2.3\ 10^{-2}$
	x_0(mm)	0.018	-0.631	-0.642
	y_0(mm)	0.403	4.803	0.957
	s_{Xo}(mm)	$9.9\ 10^{-5}$	$7.0\ 10^{-4}$	$2.3\ 10^{-4}$
	s_{Yo}(mm)	$1.3\ 10^{-4}$	$4.7\ 10^{-4}$	$3.4\ 10^{-4}$
	q(°)	0.11	1.42	89.84
	s_q(°)	$5.7\ 10^{-3}$	$8.5\ 10^{-3}$	$1.2\ 10^{-2}$
	r^2	0.9999921	0.9999899	0.9999445
	$Dz_{RESIDUAL}$(mm)	$1.076\ 10^{-3}$	$3.062\ 10^{-3}$	$2.484\ 10^{-3}$

Möller-Wedel radioscope measurement: **R_B= 202.7±1mm**

R_C= 158.0±1mm

Fig. 7.3.6d: Measured surface topographies and residuals: sample P45075B,G90 tilt.

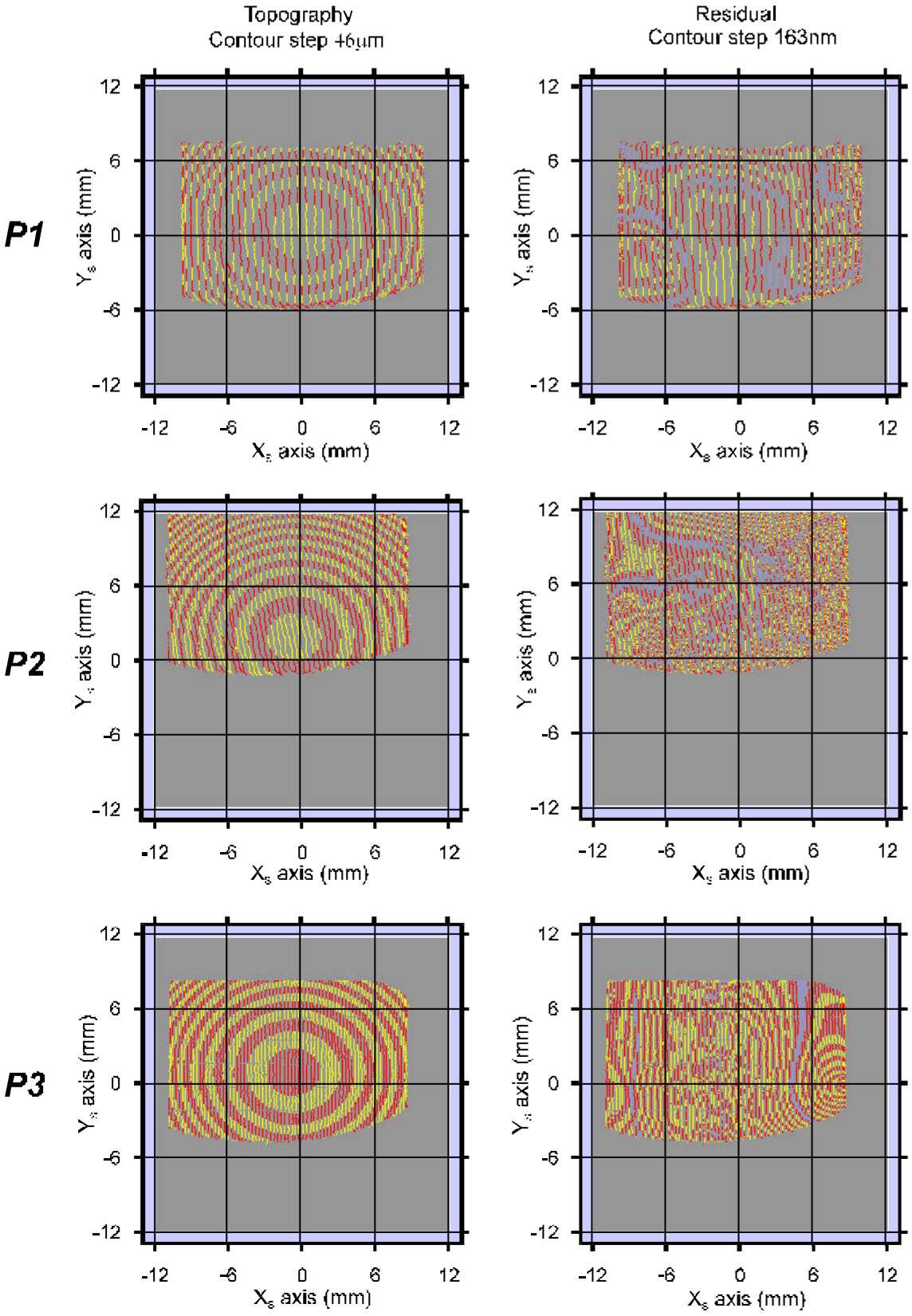

7.3.2.- Data analysis

In this final section of our experimental work, a global comment on topographic and residual plots, together with radius of curvature fitting measurements, will be presented prior to giving detailed account of each single parameter.

When extracting conclusions on the wide set of experiments presented along Section 7.3.1, we believe that the main one is the stability and reliability of the surface topographies obtained, regardless the position and orientation of the sample. This has been the main reason for the presentation of such a big number of measurements in the present work. In all cases the radius of curvature values obtained are independent, under the known experimental uncertainties, of the position and orientation of the sample, yielding stable radius of curvature measurements both through three-dimensional or two-dimensional fitting techniques. Maximum deviations of the radii values obtained in both types of measurements attain typical values of 0.4mm.

Deviations when comparing the two radius of curvature values measured using the Ronchi test with the ones measured using the radioscope are bigger, but still never fell more than a 1% outside the uncertainty limits of the radioscope measurements. Nominally identical samples present slight variations in their radius of curvature values, that may be measured repetitively using the Ronchi test technique.

In samples P30025A, P30025B, P30050A and P30050B, residual plots present the same degree of quality obtained in spherical samples. Very small total residual deviations from the best fit spherocylindrical surface are attained. Sub-micrometric surface features may be seen to rotate in the same amount as the sample when it is rotated, a feature that is easily seen when comparing residual plots at different tilts for a given sample. In particular, measurements carried out in the G00 and G90 positions present residuals that may be seen to be placed along orthogonal directions. Repetitive sub-micrometric surface differences are easily appreciated when measuring lenses nominally identical to the ophthalmic industry.

However, the quality of the residual plots may be seen to degrade to some extent in the last two samples. Although in samples P30025A, P30025B, P30050A and P30050B the quality of the residuals of the topographic reconstruction after the three-dimensional fitting procedures attains a very good quality and repetitivity, some experiments in the P45075A and P45075B samples present lower quality residuals, although the radius of curvature values obtained are as reliable and repetitive as in the remaining samples. The effect is much more visible in the P45075B sample. Notice the

contour steps in the P45075A and P45075B samples are much bigger than the ones in the remaining samples. This conclusion is confirmed by the fact that integration procedures for these two samples yielded computed residual sums much bigger than the ones attained in the remaining samples.

Adequate topographies together with not so adequate residual plots mean that the accuracy achieved along the integration procedure has degraded to some extent, yielding a surface not as smooth as the one attained in other samples. It also may be observed how even in these samples the G30 and G60 orientations present better results for the residual plots than in the G00 or G90 plots. Even in the cases of G00 and G90 plots of the P45075A and P45075B plots, better residual plots are always attained when the number of data points involved is more important (better reconstructions are achieved at the P3 distance rather than at the P1 distance).

The effect is due to the different sampling obtained in the ronchigrams with ruling lines placed along X axis or along Y axis. Typical ronchigrams of the P45075A and P45075B surfaces involve just 5 bright lines in one position of the ruling and 18 when the ruling lines are placed orthogonally in the G00 and G90 tilts. The integration algorithms used need a sampling where neighboring data points are close to each other, and they do work better with samplings of the surface equivalent (or almost equivalent) in all directions. In the G30 and G60 plots the ronchigrams present tilted shadows and the sampling of the surface happens to be more uniform, so the integration procedures perform adequately and the results obtained are quite better along these two orientations. An additional error source in ronchigrams with a very small number of bright fringes is caused by the fact that, in that case, the fringes are quite wide (typically around 60-70 pixels), which implies a higher uncertainty in the determination of the fringe centers through the eroding step. As a consequence, the uncertainty in the measured slope value becomes larger and the topographic reconstruction may be not so accurate as in other samples.

These problems could be easily avoided through minor modifications either in the experimental setup or in the measurement procedures. As a sampling as uniform as possible along orthogonal directions is to be attained, a rotating plate where positioning the sample with its principal meridians in a wider set of angles from the direction of the lines of the ruling was possible should be built. This would allow positioning the sample in the angular position where the directional effects introduced by the different magnifications of the surface along orthogonal directions would be

minimized. An alternative solution is to perform “custom” microstepping procedures for each measuring sample, that is, increasing the number of steps along that direction where the number of visible bright lines was smaller, in order to provide a more uniform sampling. Using a better software algorithm, independent of such effects, in the integration procedure should also be considered.

The numerical parameters calculated also present interesting features. The number of data points sampled experiences strong variations when tilting the sample if the principal meridians of the surface have quite different radius of curvature values. In such samples, when the principal meridians are placed along the direction of the lines of the ruling, a very different number of bright lines may be observed in each position of the ruling. When the sample is tilted so principal meridians are not coincident with the direction of the lines on the ruling, the difference in the number of lines along each direction reduces, increasing the number of visible bright lines, yielding the aforementioned more uniform sampling of the surface. Once processed, each of these new bright lines will yield a set of data points when intersected with a processed bright line of the ronchigrams with ruling lines placed in the orthogonal direction.

Sampled areas are bigger in the case of G30 and G60 samples mostly because of the area calculation procedure. Sampled areas were calculated through direct multiplication of the X and Y measured height ranges, although the defined rectangle was not completely filled with sampled data. This is caused by the fact a toroidal wavefront is registered using a rectangular CCD array, which yields a diamond-shaped pattern of data points. The increase in the measured height range in the G30 and G60 tilts is due to the possibility to obtain measurements at points which are more distant from the surface vertex at given directions, along major diagonal lines of the diamond-shaped figure obtained.

Although the area variation at the different distances may be seen to follow the same guidelines as in spherical samples, reducing as the distance from the surface to the Ronchi test increases, in samples P45075A and P45075B the measured height range does not follow these guidelines. The cause is again the lack of reliability of the integration procedures in such samples, which yields some data points at the edges of the field of view at incorrect height coordinates.

Two-dimensional fitting procedures, which may be performed independently of any integration procedure, are easily achieved in toroidal surfaces by obtaining the slope against position values along the directions where the principal meridians are

theoretically placed. Three-dimensional fitting results will show these theoretical angular positions are quite close to the real values measured on the sample. This can also be appreciated from the very good correlation coefficients of the linear fitting procedures, which show we are very close to a circular section. In fact, the two-dimensional correlation coefficients may be seen to degrade to some extent when the measured angular tilts of the sample, measured in three-dimensional fitting procedures, are bigger than 1° apart from the theoretical angular value. In these cases the section of the toroidal surface used in two-dimensional fitting procedures is 1° apart from the real circular section of the surface. The worst r^2 coefficient obtained (r^2=0.99988 in sample P30050B, G30 tilt) corresponds to the maximum measured deviation from the theoretical angular value, which is of 3.83° in this case. No relevant effect on the correlation coefficient of the position or the orientation of the sample surface has been observed.

No trend may be appreciated in the angular misalignment error term when varying either the position or the orientation of the sample. Either displacement or rotation of the sample introduces non-controlled decentering or tilt effects, which depend on how close is the vertex of the sample and the rotation axis of the sample to the optical axis of our system. An incidental interesting result may be seen in sample P30050B, G60 tilt, which presents the smallest angular misalignment values along all positions, showing it was adequately placed in the experimental setup.

This lack of observed trends is confirmed when looking at the measured coordinates of the vertex of the surface in that case, obtained through three-dimensional fitting. Taking all samples into account, typical values are, as angular misalignment ones, unpredictable as they depend on how the sample is positioned relative to the incident wavefront. Small misalignment, tilt or decentering errors will carry on noticeable variations of the measured position of the vertex of the surface when the sample is displaced or tilted. In the aforementioned sample P30050B, G60 tilt, they also come to be the smallest in all measured samples. Standard deviations for the coordinates of the vertex of the surface stay comparable in all samples, degrading to some extent in some positions in samples P45075A and P45075B.

Standard deviations for the three-dimensional fitting of radius of curvature stay in the micrometer range in the vast majority of samples and orientations, which is in good agreement with the very good correlation coefficients obtained. Again samples P45075A and P45075B, specially in its G90 orientation, may depart from this result in

some cases due to the sampling problems in the integration procedures, which prevent us from reaching the same quality in the topographic reconstruction of other samples. The numerical results this carries on are the higher standard deviations for the measured radius of curvature values, poorer correlation coefficients and bigger residual ranges that appear in some cases in these samples. Those big residual range values, however, are only attained by independent data points, usually placed at the edge of the field of view, which were not adequately integrated. It must be noticed how the bigger standard deviations correspond to the cross curve, as this is the curve which has less data available in the G00 and G90 positions (only 5 bright lines are visible in the field of view in samples P45075A and P45075B, for instance).

The remaining parameter of our fitting procedures, the measured angular position of the principal meridians of the toroidal surface, is fully consistent with the theoretical value fixed in our experimental setup. This proves how the direction of the principal meridians may also be accurately measured regardless the position and orientation of the sample. Some G90 tilts present θ values around 0°, and some G00 values close to 90°, following our previous definition of θ as the angle where one principal meridian could be found in the first quadrant. The quality of the fitting and the small standard deviation involved allow us to ensure we are adequately measuring both the radius of curvature of the toroidal surface and the direction where they are placed.

As a summary, reliable and repetitive measurements of radius of curvature have been attained in toroidal surfaces, yielding an accurate determination of the radius of curvature of the surface and of the angular position where the principal meridians are placed. Topographic measurements and residuals from the best fit spherocylindrical surface have also been attained regardless the position and orientation of the sample. Sub-micrometric surface features may be seen to tilt when the sample surface is tilted. When the radius of curvature values present strong differences (over 0.75D of power difference between both meridians of the surface, which amounts a 25% difference in radius of curvature values) further improvements to the technique need be considered in order to distribute all sampling points as uniformly as possible on the surface, due to requirements of the integration algorithm used. Otherwise, the quality of the residual plots obtained is degraded to some extent, although the topographic measurements obtained allow accurate measurements of all the surface parameters, yielding larger standard deviations for the measured data.